Nano Research

Open Access

Research Article

Photoinduced rapid-deposition of wafer-scale high-density semiconducting single walled carbon nanotube networks for thin-film transistors

Shangjing Yang[1,§] ✉, Zidong Tu[2,§], Rui He[1], Shuqing Cao[1], Feige Yu[2], and Yu Xia[1,3,4] ✉

[1] *Key Laboratory for the Physics and Chemistry of Nanodevices and Center for Carbon-based Electronics, School of Electronics, Peking University, Beijing 100871, China*
[2] *Departments of Hunan Institute of Advanced Sensing and Information Technology, Xiangtan University, Xiangtan 411105, China*
[3] *Institute of Carbon-Based Thin Film Electronics, Peking University, Taiyuan 030012, China*
[4] *Institute of Advanced Functional Materials and Devices, Shanxi University, Taiyuan 030006, China*
[§] *Shangjing Yang and Zidong Tu contributed equally to this work.*

Cite this article: *Nano Research*, **2026**, *19*, 94908335. https://doi.org/10.26599/NR.2026.94908335

ABSTRACT: Semiconducting single walled carbon nanotubes (s-SWNTs) have shown great promise in a variety of thin-film transistor (TFT) applications. Although several solution processing techniques have resulted in high-quality s-SWNT network films, exquisite control of film morphology at wafer-scale to achieve desired s-SWNT density and uniformity remains challenging. In addition to this hurdle, there is the slow s-SWNT absorbing dynamics in large-scale fabrication schemes that require several hours to days to complete. Here, we report a photoinduced rapid-deposition technique to prepare wafer-scale s-SWNT films. Leveraging the tendency for azo-benzene materials to preferentially migrate to substrate surface under light, we utilized a light-sensitive polymer poly[(9,9-dioctylfluorenyl-2,7-diyl)-alt-co-(4,4'-azobenzene)] (PFNAB) to wrap s-SWNTs and accelerate s-SWNT deposition. s-SWNT networks prepared from this method afford films with high-density (> 50 s-SWNTs per micrometer) and high-uniformity across a 4-inch wafer. More importantly, the deposition can be completed within 30 min. Field-effect transistors (FETs) comprising these s-SWNT films as active layers exhibit an on-state current of 2.44 μA·μm^{-1} at source–drain voltage of −1 V (V_{ds} = −1 V), which is among the highest values in reported field-effect transistors with s-SWNT network films for TFT applications. This new photo-deposition technique is amenable to new application possibilities in s-SWNT TFT electronics.

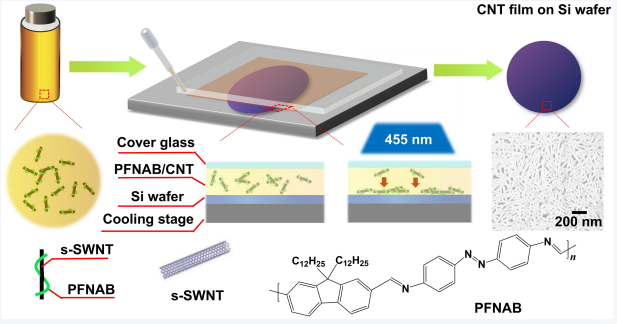

KEYWORDS: single walled carbon nanotubes, photoinduced deposition, wafer-scale, thin-film transistors

1 Introduction

Spurred by the success in the digital display industry, thin-film transistors (TFTs) are now ubiquitously seen in the emerging applications from flexible and printed electronics, digital detectors, to integrated circuits [1–3]. Although various types of semiconductors have been employed in TFTs, including polycrystalline silicon [4], cadmium selenide [5], metal oxides [6], organic semiconductors [7], and semiconducting single walled carbon nanotube (s-SWNT), s-SWNT is advantageous because of its exceptional charge transport properties, outstanding mechanical flexibility and robustness, mild processing condition and chemical resilience [8–10]. Furthermore, thanks to its low temperature processability, s-SWNT can be facilely solution-processed by spin coating, electrophoretic deposition, vacuum filtration, spray coating, direct solution deposition, and dip coating [11–14]. Such methods, whether accomplished by non-equilibrium transition with fast solvent removal or slow adsorbing dynamics of s-SWNT to a substrate surface, are able to produce high-quality films comprising high-density s-SWNT network, the incorporation of which has resulted in high-performance electronics [15]. However, scaling these processing schemes from lab-scale demonstration to produce

Received: October 14, 2025; **Revised:** December 5, 2025
Accepted: December 11, 2025

✉Address correspondence to Shangjing Yang, 2201111415@stu.pku.edu.cn; Yu Xia, yu_xia@pku.edu.cn

applications-relevant and wafer-scale quantities of s-SWNT films remains challenging. Traditional rapid processing methods, such as spin coating, vacuum filtration, and spray coating, although convenient in preparing inch-scale films, often suffer from poor uniformity due to their non-equilibrium transition nature during fast solvent removal processes [16]. In comparison, electrophoretic deposition offers relatively better film uniformity [13]. However, it requires meticulous control over multiple parameters, making the entire process extremely sensitive to external conditions; any deviation can easily introduce defects. Direct solution deposition and dip coating are the most successful preparation methods for wafer-scale s-SWNT films so far [12]. These methods promise to produce s-SWNT films with desired density, large-area uniformity, and minimized defect density, though this promise comes at the expense of fabrication efficiency: The slow adsorbing dynamics of s-SWNT in these techniques make the deposition time-consuming, often requiring several hours to days to achieve desired high-density and uniformity. There is thus a pressing demand to develop a rapid deposition method for wafer-scale high-quality s-SWNT films targeting for industry-level TFT applications.

Herein, we introduce a novel photoinduced deposition technique to prepare wafer-scale SWNT films with uniform s-SWNT density. We utilized a photo-sensitive polymer poly[(9,9-dioctylfluorenyl-2,7-diyl)-alt-co-(4,4'-azobenzene)] (PFNAB) to wrap s-SWNTs and disperse them in toluene, followed by a photoinduced deposition process, in which visible light was employed to accelerate s-SWNT deposition onto target substrates. This technique leverages the light-sensitive property of azobenzene molecules: When exposed to light, molecules bearing azobenzene moieties absorb light and migrate to the interface of target substrate [17]. Such technique has been widely applied in the liquid crystal display industry [18, 19]. Our approach distinguishes itself through three key advancements: First, the light-driven migration mechanism of azo-benzene molecules enables much faster deposition of PFNAB-wrapped s-SWNTs, allowing uniform coating of s-SWNTs on 2- and 4-inch wafers within 30 min with a density of 50 s-SWNTs·μm^{-1} and a small density variation of 5.08%. This performance surpasses the coating efficiency and effectiveness of the conventional direct solution deposition and dip-coating methods. Second, this process is highly efficient in material usage, consuming merely 5 mL of s-SWNTs solution to coat an entire 4-inch wafer, which is considerably more economical compared to many large-scale coating techniques. Third and crucially, unlike immersion-based methods that often lead to the undesirable formation of s-SWNT films on both sides of the substrate, our photoinduced process enables selective, single-sided deposition. This feature is vital for many electronic applications as it effectively prevents potential current leakage or parasitic channels caused by backside nanotubes, thereby simplifying device integration and enhancing device performance and reliability. Field-effect transistors (FETs) with these high-density s-SWNT films as active layers exhibit an average on-state current of 2.44 μA·μm^{-1} at source–drain voltage of −1 V (V_{ds} = −1 V) and a current on/off ratio higher than 10^5. This new photo-deposition technique of s-SWNT films thus opens up new application possibilities in s-SWNT TFT electronics.

2 Results and discussion

Figure 1 depicts the light-induced deposition scheme of s-SWNT utilizing the azo-benzene polymer PFNAB. Purification of s-SWNT by PFNAB was carried out in toluene solution following Ref. [20]. s-SWNT purity after sorting is confirmed by ultraviolet–visible (UV–Vis) spectrum to be higher than 99.9% (Fig. S1 in the Electronic Supplementary Material (ESM)), adequate for TFT application. As shown in Fig. 1, a unit cell was constructed by a silicon wafer with a quartz substrate separated with a controlled gap of approximately 1 mm with a polyimide spacer. s-SWNT dispersion was then injected via capillary force. A blue light with a wavelength of 455 nm was employed to induce the *trans*-to-*cis* isomerization of the azobenzene-containing PFNAB molecules, which effectively alters the polarity of PFNAB, thus driving PFNAB and PFNAB/s-SWNTs diffusing towards interfaces [21]. The *cis*-isomer of PFNAB, characterized by a significant dipole moment, exhibits greater polarity and distinct chemical potential compared to the *trans* structure [22]. Given that the chemical environment at the solid–liquid interface favors the accumulation of polar species [23], upon irradiation, a concentration gradient of the *cis*-isomer forms from the solution toward the interface [24]. This gradient promotes diffusion, thereby driving the transport of PFNAB/SWNTs toward the interface and leading to rapid adsorption. Based on this mechanism, light is used in our setting to accelerate s-SWNT deposition over large area using a uniform-irradiating lamp. The scanning electron microscopy (SEM) image in Fig. 1 shows a high-density SWNT network film at the end of the deposition process.

To unequivocally validate the proposed light-driven deposition

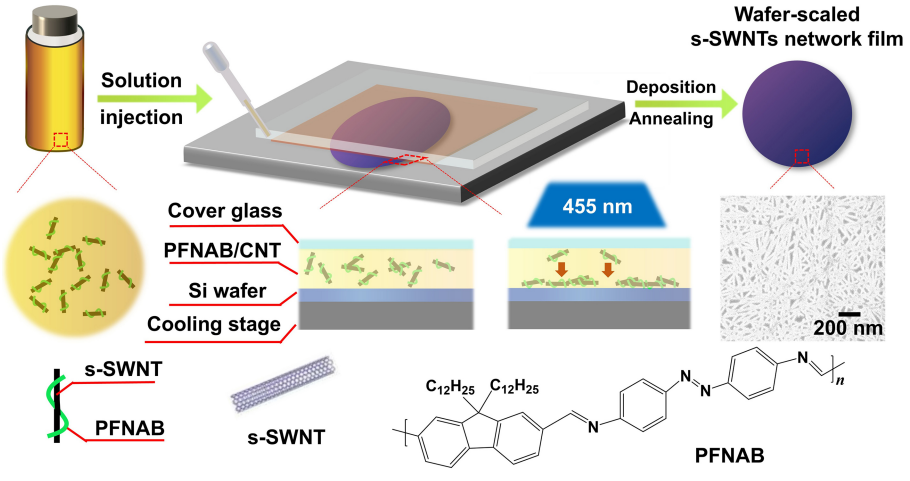

Figure 1 Schematic illustration of the photoinduced deposition setting.

mechanism and distinguish the unique role of PFNAB, we designed a well-conceived mechanistic experiment (for detailed setup, see Section 4 and Fig. S9 in the ESM). Briefly, three elongated vials were filled with an equal volume of polymer/s-SWNT solution. Vials in Groups A and B contained PFNAB as the wrapping polymer, while Group C used poly[n-(1-octylnonyl)-9h-carbazole-2,7-diyl] (PCz), a non-photoactive polymer reported elsewhere for reference. Groups A and C were irradiated from the bottom with a 455 nm light source, whereas Group B (PFNAB-wrapped s-SWNTs) was kept in the dark as a control. After 4 h of irradiation, the solutions were sampled from five distinct vertical positions for UV–Vis spectroscopy. The results, summarized in Fig. S9 in the ESM, show that only Group A (PFNAB, under light) exhibits a significant, gradient change in the s-SWNT absorption peak intensity from the top to the bottom of the vial. This observation confirms that PFNAB-wrapped s-SWNTs undergo phototactic aggregation towards the light source under 455 nm irradiation. In contrast, the absence of such a gradient in the control groups (Group B without light and Group C with a different polymer) rules out the possibility of sedimentation being the primary cause and highlights the indispensability of both the azobenzene moiety in PFNAB and the light stimulus. This experiment provides evidence for the light-driven directional migration of PFNAB/s-SWNT complexes, which is the cornerstone of our rapid, uniform deposition technique.

To determine the optimal wavelength for photoinduced deposition, we first characterized the light absorption property of PFNAB using UV–Vis spectroscopy. As shown in Fig. 2(a), PFNAB in toluene exhibits an absorption peak at approximately 420 nm. Upon irradiation with 455 nm blue light, the photoisomerization of *trans*-azobenzene to *cis*-azobenzene reduces the peak intensity in the UV–Vis spectra (Fig. 2(a)). However, since most PFNAB molecules are physically bonded with s-SWNT, the photo-isomerization is partially constrained, resulting in only a minor intensity decrease even after 20 min of light irradiation. Here, for safety considerations, we selected 455 nm blue light (slightly longer than PFNAB's peak absorption at 420 nm) as the excitation source. Despite this wavelength offset, the light remains sufficiently effective to drive the deposition of PFNAB-wrapped s-SWNTs onto the target substrate (Fig. 3).

We then studied the density of the deposited s-SWNT films under various deposition conditions, including s-SWNT solution concentration, light intensity, and deposition time (Figs. 2(b)–2(d)). For these systematic investigations, when one parameter was varied, the other two were fixed at their optimal or a standard value. Specifically, the concentration-dependent study (Fig. 2(b)) was conducted with a fixed light intensity of 130 mW·cm^{-2} and a deposition time of 40 min. The light power-dependent study (Fig. 2(c)) employed a fixed s-SWNT concentration of 30 μg·mL^{-1} and a deposition time of 40 min. Lastly, the time-dependent study (Fig. 2(d)) was performed with a fixed s-SWNT concentration of 30 μg·mL^{-1} and a light intensity of 130 mW·cm^{-2}. In a typical setting of depositing s-SWNT film on a 2-inch silicon wafer, we observe a substantial increase in s-SWNT density from 22 ± 3 to 51 ± 2 counts·μm^{-1} when s-SWNT solution concentration is elevated from 5 to 30 μg·mL^{-1}. However, increasing the concentration further to 40 μg·mL^{-1} yields only a marginal improvement in density. Similarly, the highest s-SWNT density is achieved with the highest light irradiation intensity of 130 mW·cm^{-2} and the longest deposition time of 40 min in our testing schemes, respectively (Figs. 2(c) and 2(d)). Representative SEM images corresponding to the data points in Figs. 2(b)–2(d) are provided in Figs. S10–S12 in the ESM, respectively. It is relatively intuitive that higher s-SWNT solution concentration, higher light irradiation intensity, and longer

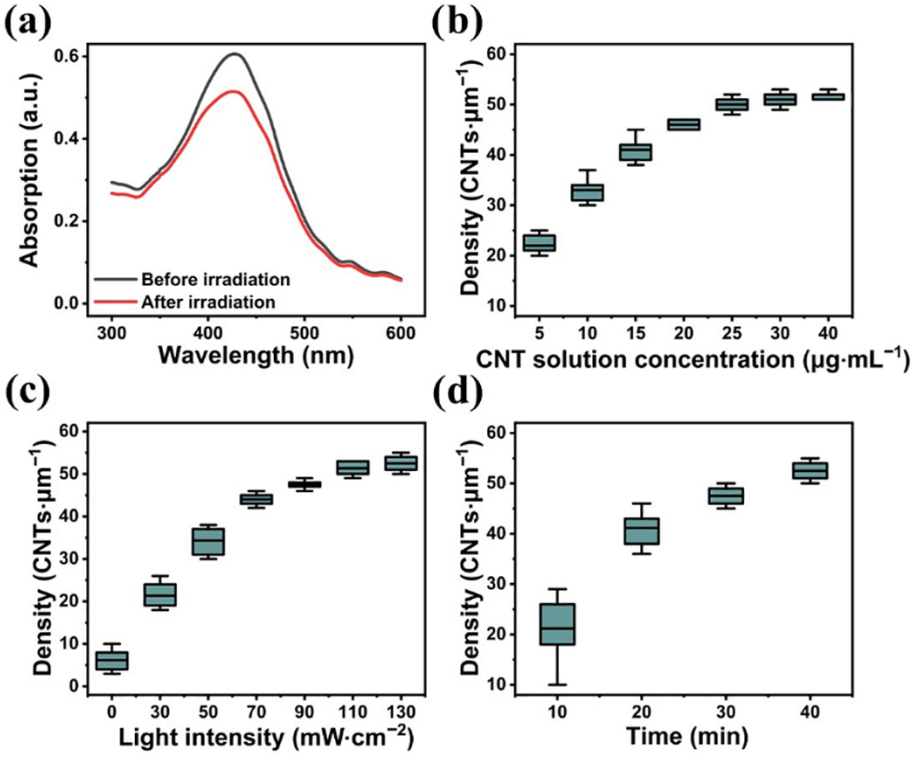

Figure 2 Study of deposition conditions. (a) UV–Vis spectra of PFNAB before and after irradiation with a 455 nm blue light. ((b)–(d)) Deposition density of s-SWNT films (s-SWNTs·μm^{-1}) under different deposition conditions: (b) s-SWNT solution concentration, (c) light intensity, and (d) deposition time.

deposition time promote more s-SWNTs depositing onto the target substrate, because the number of s-SWNTs migrating to the substrate generally increases with higher s-SWNT concentration, light intensity, and deposition time, though the relationship is not strictly linear, as shown in Fig. 2. However, it should be noted that although further increase of s-SWNT solution concentration, light irradiation intensity, or deposition time would lead to slightly higher s-SWNT density, according to our findings in Figs. 2(b)–2(d), such minor enhancement of density would be insignificant to have a meaningful impact on FET performance due to the complexity of device fabrication. Therefore, we determine the optimal deposition conditions for our system to be s-SWNT solution concentration of 30 μg·mL^{-1}, light irradiation intensity of 110 mW·cm^{-2}, and deposition time of 30 min. In a sharp contrast, direct deposition of s-SWNT without light irradiation yields only sparse adsorption of carbon nanotubes on the substrate (Fig. S2 in the ESM). After s-SWNT deposition, PFNAB was then successfully removed through a thermal annealing process at 600 °C for 60 min to ensure a reliable contact in later FET fabrication (Fig. S3 in the ESM).

Large-scale uniformity of the s-SWNT network film is vital for s-SWNT FET preparation in TFT applications. We employed SEM and polarized Raman spectroscopy to evaluate the uniformity of the s-SWNT film, as shown in Fig. 3. SEM data shows a consistent density of approximately 50 s-SWNTs·μm^{-1} across all regions, with a variability of 5.08% (Figs. 3(b) and 3(c) and Figs. S5 and S6 in the ESM), further underscoring the uniform distribution of the s-SWNT network film over the whole wafer. Atomic force microscopy (AFM) images in Fig. S13 in the ESM also reveal the homogeneous morphology and uniform distribution of the s-SWNT network at the nanoscale over a large area. The consistent network density observed in these images further corroborates the high uniformity of the film, as quantified by the SEM density statistics in Fig. 3(c). When compared to alternative deposition methods from literature (Fig. 3(d)), our technique presented herein not only achieves superior s-SWNT density but also significantly shortens the deposition time. Figure 3(e) illustrates the Raman spectra of a s-SWNT film at various polarized angles ranging from 0° to 180°. After normalization of the absorption spectra with respect to the Si peak at 520.7 cm^{-1} (Fig. 3(e) and Fig. S4 in the ESM), the s-SWNT absorption peak at 1600 cm^{-1} Raman shift exhibits consistent intensity across all polarization angles. This

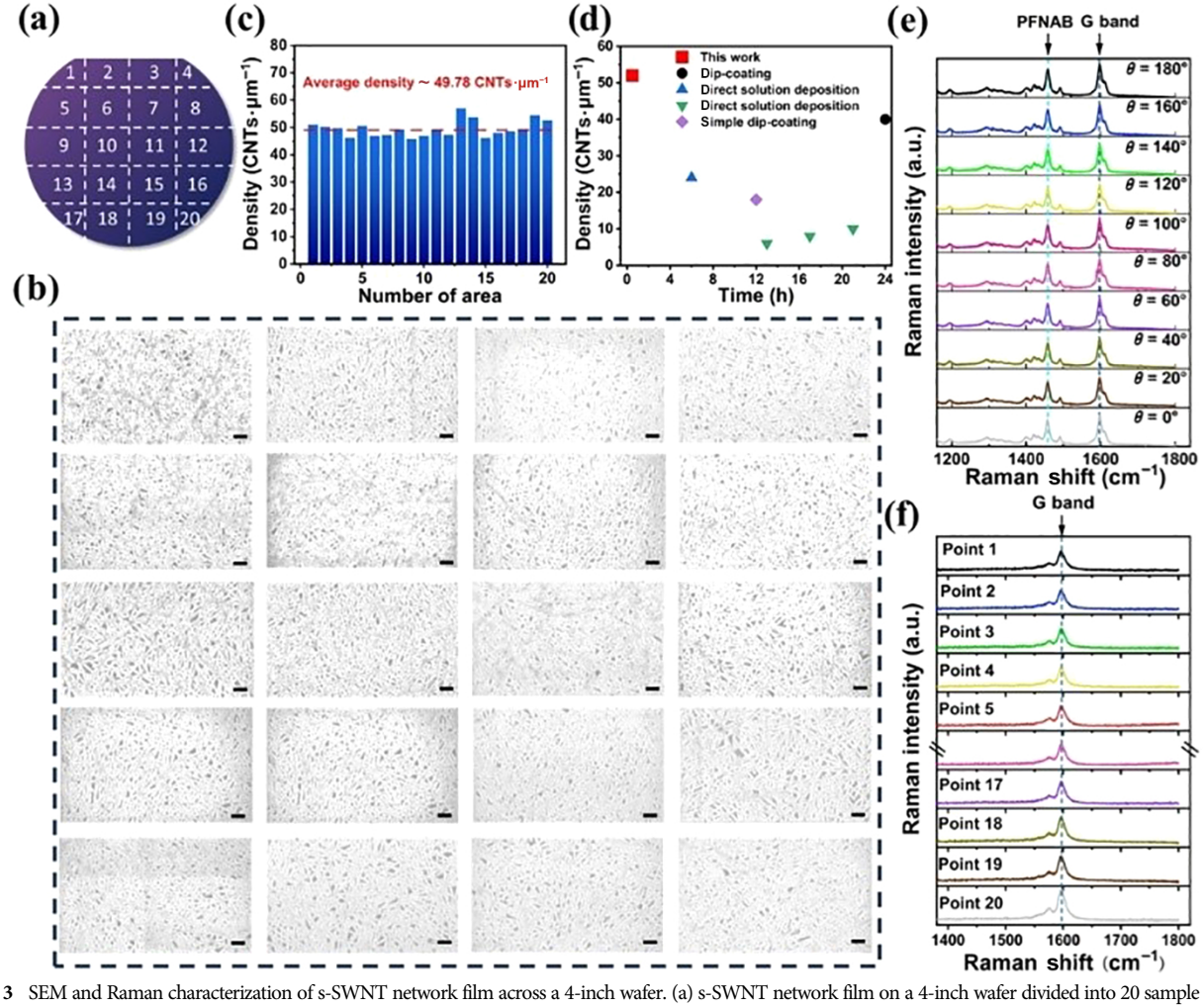

Figure 3 SEM and Raman characterization of s-SWNT network film across a 4-inch wafer. (a) s-SWNT network film on a 4-inch wafer divided into 20 sample areas for wafer-scale characterization. (b) SEM images of s-SWNT film, obtained from 20 different areas across the 4-inch wafer sample. Scale bar: 200 nm. (c) Summary of s-SWNT density in 20 sample areas measured from SEM images shown in (b). (d) Plot of carbon nanotube density vs. preparation time for various s-SWNT network film preparation methods [25–28]. (e) Polarized Raman spectra of s-SWNT films at various polarizer angles from 0° to 180°. (f) Raman spectra collected from 20 randomly selected spots across the 4-inch wafer sample, with each spot chosen from a distinct domain as shown in (a). Dash line represents the position of G band.

result signifies the successful formation of an isotropic, uniform s-SWNT network through the PFNAB photoinduced deposition process. Furthermore, we performed Raman analysis at 20 different sample areas across a 4-inch wafer, as shown in Fig. 3(f). Raman analysis of the G band of s-SWNT at these sample areas reveals a uniform density distribution across wafer scale (Fig. S7 in the ESM). These position our technique as a highly effective and expedient approach for s-SWNT network deposition, offering substantial improvements for the fabrication of uniform and high-performance FETs.

Armed with the high-density and uniform s-SWNT network material, we then fabricated s-SWNT network FETs in a top-contact and back-gate architecture. FETs were fabricated following the process shown in Fig. 4(a). s-SWNT network film was initially photo-deposited onto the top thermally grown silicon dioxide (SiO_2) layer of a heavily doped silicon substrate. In this setting, the SiO_2 layer acts as both the deposition substrate of s-SWNT film and the gate dielectric of the FET. A dual-layer photoresist system comprising S1813 and LOR 3A was used in the photolithography process to enable effective metal lift-off and achieve improved patterning resolution. Source and drain contacts (Ti/Pd/Au, 0.3/30/60 nm) were then deposited by electron beam evaporation. The composition and deposition structure of the contact metal are meticulously engineered to establish a high-quality, low-resistance Ohmic contact with the p-type s-SWNT channel. Figure 4(b) confirms the successful preparation of the FET, showing minimal change in both the morphology and density of the s-SWNT network within the channel. The output curves (Fig. 4(c)) show that the drain current increases linearly with drain voltage at low V_{ds}, a confirmation of good Ohmic contact. This lack of a significant non-

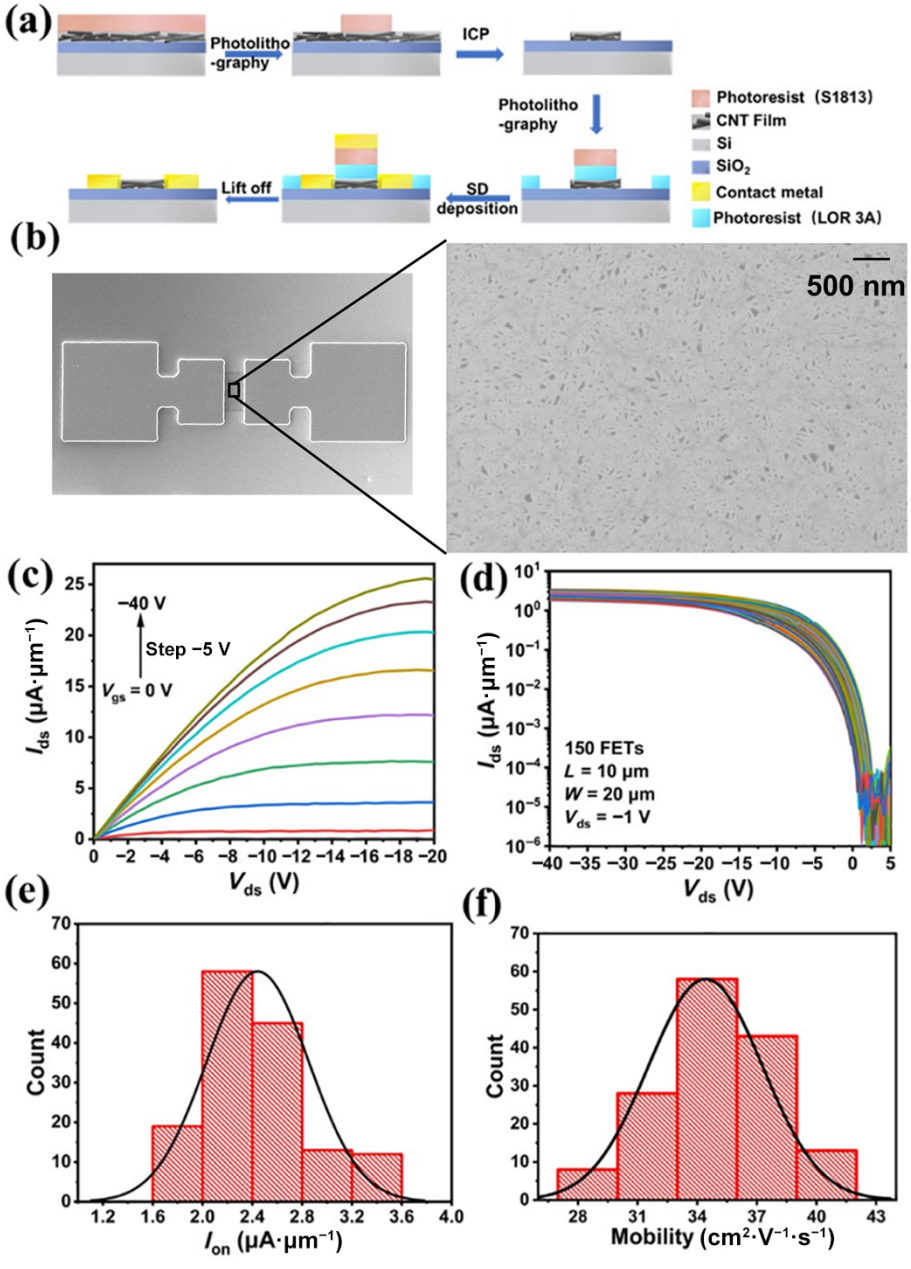

Figure 4 FET fabrication and characterization. (a) Fabrication process of top-contact and bottom-gate FETs. (b) SEM images of device structure and s-SWNT channel. (c) Output characteristic curves at different V_{gs}. (d) Transfer curves of 150 FETs. (e) The I_{on} distribution. (f) The mobility distribution.

linear turn-on voltage at the origin signifies that charge injection from the electrode is efficient and not a primary limiting factor for device performance. Figure 4(d) displays drain current vs. gate voltage (I_{ds}–V_{gs}) characteristics of 150 s-SWNT network-based FETs. The source–drain bias was set at −1 V, and the gate bias was swept from −40 to 5 V. These I_{ds}–V_{gs} curves exhibit p-type behavior of s-SWNT FETs, with an average on-state current of 2.44 μA·μm^{-1} with only ± 0.41 μA·μm^{-1} current variation (less than 17% variation shown in Fig. 4(e)). Similarly, subthreshold swing (SS) and carrier mobility also show decent performances with narrow distributions of 0.42 ± 0.02 V·dec^{-1} and 34.41 ± 2.86 cm^2·V^{-1}·s^{-1}, respectively (Fig. 4(f) and Fig. S8 in the ESM).

Moreover, on–off ratio of more than 80% FETs exceeds 10^5 (Fig. S8 in the ESM). The distribution of the on-state current (I_{on})/off-state current (I_{off}) ratio, as shown in Fig. S8(c) in the ESM, fails to follow a perfect normal distribution but rather exhibits a right-skewed distribution. This metric is highly sensitive to minor variations in the I_{off}. The off-state current itself is influenced by a multitude of factors, including the presence of residual metallic s-SWNTs, tunneling currents through the gate dielectric, and the percolation transport characteristics within the s-SWNT network. Therefore, the skewed distribution effectively reflects the collective impact of spatial inhomogeneities on the most sensitive performance metric, while the fact that over 80% of devices still achieve a ratio > 10^5 underscores the high overall quality and uniformity of our s-SWNT network.

These device metrics thus place our s-SWNT FETs among the best-performing FETs with s-SWNT network films as the channel material (Fig. S8 in the ESM and Table 1). It should be noted that compared to a variety of previous studies detailed in Table 1, our work demonstrates s-SWNT FETs with much improved electronic performances with superior uniformity, which is deeply rooted in the high-quality s-SWNT material prepared by our unique deposition technique.

3 Conclusions

In this work, we introduce a photoinduced rapid-deposition method for the fabrication of high-density and wafer-scale uniform s-SWNT network films as channel materials for high-performance FETs. The approach utilizes an innovative azobenzene-based polymer (PFNAB) to selectively wrap s-SWNTs, enabling their uniform deposition onto a 4-inch silicon wafer within 30 min to form a high-density, well-distributed carbon nanotube network film.

The resulting FETs, incorporating this s-SWNT network thin film as the channel, achieve a remarkable uniformity in device performance across wafer-scale, delivering an on-state current density of 2.44 μA·μm^{-1} and an on/off ratio higher than 10^5. This technique offers a promising solution for next-generation s-SWNT-based TFT electronics.

4 Experimental section

4.1 Purification of carbon nanotube

60 mg of Arc-discharge SWNTs (carbon solutions) and 60 mg of polymer (PFNAB) were added into 120 mL toluene (high-performance liquid chromatography (HPLC)). Ultrasonication (JY92-IIDN) was performed at 450 W for 40 min, followed by 330 W power for 60 min in an ice water bath. The mixture was then centrifuged at 19,000*g* (Sigma 3K15) for 1 h. Following centrifugation, 90% of the supernatant was retained as the original solution for next deposition process. The purity of s-SWNTs in this solution was quantified using UV–Vis spectroscopy (SHIMADZU UV-3600i PLUS).

4.2 Preparation of s-SWNT network film

The distance between target substrate and the upper quartz plate was fixed at around 1 mm using a spacer. The s-SWNT/PFNAB solution was injected from the side until the interlayer was filled. Then the distance between the light source and the deposition cell was adjusted until the light intensity on the surface of the cell reached 110 mW·cm^{-2}. The deposition was maintained for 30 min with a semiconductor refrigeration plate (XD-6028). Then the upper quartz plate was released, followed by rinsing of the substrate with toluene and isopropyl alcohol (IPA) for 1 min, respectively. The substrate was then dried with a nitrogen gun and baked on a hot plate at 150 °C for 5 min to enhance the bonding strength

Table 1 Performance comparison of large-area s-SWNT network film devices

FET information	I_{on} (μA·μm^{-1})	I_{on}/I_{off}	Mobility (cm^2·V^{-1}·s^{-1})	Gate/gate dielectric	References
L = 10 μm, W = 20 μm, 150 devices measured	2.44 (average)@V_{ds} = −1 V	> 10^5 (~ 80% devices) and > 10^6 (~ 20% devices)	34.41 (average)	Si/SiO_2 (100 nm)	This work
L = 5 μm, W = 10 μm, 210 devices measured	1.09 (average)@V_{ds} = −1 V	> 10^5 (74.76% devices)	31.78 (average)	Metal/HfO_2 (20 nm)	[29]
L = 5 μm, W = 50 μm, 210 devices measured	1.49 (average)@V_{ds} = −1 V	> 10^5 (73.81% devices)	37.26 (average)		
L = 50 μm, W = 100 μm, 120 devices measured	0.6–1@V_{ds} = −2 V	> 10^3 (~ 60% devices) and > 10^4 (< 20% devices)	11 (average)	Al/Al_2O_3 (20 nm)	[30]
L = 2 μm, W = 20 μm	< 0.05@V_{ds} = −0.9 V	> 10^5 (~ 52% devices) and > 10^6 (~ 14% devices)	~ 24	Si/SiO_2 (100 nm)	[31]
L = 5 μm, W = 20 μm		> 10^5 (~ 58% devices) and > 10^6 (~ 13% devices)			
L = 10 μm, W = 40 μm, 100 devices measured	0.88@V_{ds} = −0.1 V	> 10^4 (~ 80% devices)	28.97 (average)	Si/SiO_2 (300 nm)	[32]
L = 100 μm, W = 100 μm, 46 devices measured	0.2@V_{ds} = -5.1 V	> 10^5 (~ 91% devices) and > 10^6 (~ 77% devices)	20 (average)	Metal/Al_2O_3 (40 nm)	[33]
L = 50 μm, W = 100 μm, 10 devices measured	0.05@V_{ds} = −5.1 V	> 10^7 (~ 90% devices)	16 (average)	Metal/Al_2O_3 (50 nm)	[34]

between s-SWNTs and substrate. Finally, the wafer was vacuum annealed at 600 ℃ for 1 h to remove any organic residual.

4.3 Density measurement and material characterization

Morphological characteristics and spatial uniformity of the s-SWNT film deposited on a 4-inch silicon wafer were comprehensively investigated using a field-emission scanning electron microscope (SEM, ZEISS SIGMA 300) with a low acceleration voltage of 1.0 kV. 20 different positions were randomly selected to characterize the film at a magnification of 40,000×. The number of s-SWNTs at all sampling points snapped by SEM was counted by image processing software (Photoshop 2024). A straight line (1 μm in length) was drawn at an arbitrary position in each SEM image. The number of intersections between the line and s-SWNTs was then counted as the density of carbon nanotubes in the measured sample (Fig. S6 in the ESM). Raman spectra mapping of s-SWNT network films was conducted using a Horiba Jobin Yvon HR-800 confocal Raman micro-spectrometer with an excitation wavelength of 488 nm.

4.4 FET preparation

FETs of s-SWNTs were prepared with a top-contact and bottom-gate configuration. The fabrication sequence began with the definition of alignment markers. The marking area was patterned by UV exposure in proximity exposure mode with an exposure dose of 260 mJ·cm^{-2} to ensure complete development of photoresist in the following step. A 10/45 nm Ti/Au layer was then deposited via e-beam evaporation (EBE, DE400). The excess s-SWNT network film was then removed using inductively coupled plasma (ICP, TRRION TECHNOLOGY IIIICP) etching for 30 s under 500 W radio frequency (RF) power with pure O_2 gas. The source and drain electrode area was patterned using a dual-layer photoresist system of S1813 and LOR 3A. Finally, 0.3/30/60 nm Ti/Pd/Au was deposited as the source and drain metal at a rate of 0.5/0.5/2 Å·s^{-1}, respectively. The device performance was measured by a semiconductor characterization system (Keithley, 4200-A) in air.

4.5 Electrical characterization and parameter extraction

The field-effect mobility (μ) was calculated in the linear regime ($V_{ds} = -1$ V) using Eq. (1)

$$\mu = \frac{L}{W}\frac{1}{C_{ox}}\frac{g_m}{V_{ds}} \quad (1)$$

where L and W are the channel length and width, respectively, C_{ox} is the gate oxide capacitance per unit area (~ 34.5 nF·cm^{-2} for 100 nm SiO_2), and $g_m = \partial I_{ds}/\partial V_{gs}$ is the transconductance.

The SS was extracted from the transfer characteristics using Eq. (2)

$$SS = \left(\frac{\partial \log_{10}(I_{ds})}{\partial V_{gs}}\right)^{-1} \quad (2)$$

which represents the gate voltage required to increase the drain current by one decade in the subthreshold region.

Electronic Supplementary Material: Supplementary material (UV–Vis spectra of s-SWNT solution, SEM and Raman details of s-SWNT network, SS, threshold voltage and I_{on}/I_{off} ratio distribution of FETs) is available in the online version of this article at https://doi.org/10.26599/NR.2026.94908335.

Data availability

All data needed to support the conclusions in the paper are presented in the manuscript and the Electronic Supplementary Material. Additional data related to this paper may be requested from the corresponding author upon request.

Acknowledgements

We acknowledge support from the National Key Research & Development Program of China (No. 2022YFB3204401) and the National Natural Science Foundation of China (No. 52272132). We also thank Peking Nanofab for its support in device fabrication and material processing.

Declaration of competing interest

All the contributing authors report no conflict of interests in this work.

Author contribution statement

S. J. Y., Z. D. T., and Y. X. conceived the idea and designed the experiments. S. J. Y. and Z. D. T. formulated the CNT solution, fabricated the CNT network films and FETs, and performed film characterization and device testing. R. H., S. Q. C., and F. G. Y. assisted with experiments. Y. X. supervised the work. S. J. Y. and Z. D. T. analyzed the data and drafted the manuscript. S. J. Y., Z. D. T., R. H., and Y. X. revised the manuscript. All authors discussed the results and commented on the manuscript. All the authors have approved the final manuscript.

Use of AI statement

None.

References

[1] Fortunato, E.; Barquinha, P.; Martins, R. Oxide semiconductor thin-film transistors: A review of recent advances. *Adv. Mater.* **2012**, *24*, 2945–2986.
[2] Dimitrakopoulos, C. D.; Mascaro, D. J. Organic thin-film transistors: A review of recent advances. *IBM J. Res. Dev.* **2001**, *45*, 11–27.
[3] Duan, X. F.; Niu, C. M.; Sahi, V.; Chen, J.; Parce, J. W.; Empedocles, S.; Goldman, J. L. High-performance thin-film transistors using semiconductor nanowires and nanoribbons. *Nature* **2003**, *425*, 274–278.
[4] Brotherton, S. D. Polycrystalline silicon thin film transistors. *Semicond. Sci. Technol.* **1995**, *10*, 721–738.
[5] Talapin, D. V.; Murray, C. B. PbSe nanocrystal solids for n- and p-channel thin film field-effect transistors. *Science* **2005**, *310*, 86–89.
[6] Banger, K. K.; Yamashita, Y.; Mori, K.; Peterson, R. L.; Leedham, T.; Rickard, J.; Sirringhaus, H. Low-temperature, high-performance solution-processed metal oxide thin-film transistors formed by a "sol–gel on chip" process. *Nat. Mater.* **2011**, *10*, 45–50.
[7] Dimitrakopoulos, C. D.; Malenfant, P. R. L. Organic thin film transistors for large area electronics. *Adv. Mater.* **2002**, *14*, 99–117.
[8] Krupke, R.; Hennrich, F.; Lohneysen, H. V.; Kappes, M. M. Separation of metallic from semiconducting single walled carbon nanotubes. *Science* **2003**, *301*, 344–347.
[9] Cao, J. E.; Wang, Q.; Dai, H. J. Electromechanical properties of

metallic, quasimetallic, and semiconducting carbon nanotubes under stretching. *Phys. Rev. Lett.* **2003**, *90*, 157601.
[10] Li, Y. M.; Mann, D.; Rolandi, M.; Kim, W.; Ural, A.; Hung, S.; Javey, A.; Cao, J. E.; Wang, D.; Yenilmez, E. et al. Preferential growth of semiconducting single walled carbon nanotubes by a plasma enhanced CVD method. *Nano Lett.* **2004**, *4*, 317–321.
[11] Rinzler, A. G.; Liu, J.; Dai, H.; Nikolaev, P.; Huffman, C. B.; Rodríguez-Macías, F. J.; Boul, P. J.; Lu, A. H.; Heymann, D.; Colbert, D. T. Large-scale purification of single-wall carbon nanotubes: Process, product, and characterization. *Appl. Phys. A* **1998**, *67*, 29–37.
[12] Park, S.; Vosguerichian, M.; Bao, Z. A review of fabrication and applications of carbon nanotube film-based flexible electronics. *Nanoscale* **2013**, *5*, 1727–1752.
[13] Boccaccini, A. R.; Cho, J.; Roether, J. A.; Thomas, B. J. C.; Jane Minay, E.; Shaffer, M. S. P. Electrophoretic deposition of carbon nanotubes. *Carbon* **2006**, *44*, 3149–3160.
[14] LeMieux, M. C.; Roberts, M.; Barman, S.; Jin, Y. W.; Kim, J. M.; Bao, Z. Self-sorted, aligned nanotube networks for thin-film transistors. *Science* **2008**, *321*, 101–104.
[15] Arnold, M. S.; Green, A. A.; Hulvat, J. F.; Stupp, S. I.; Hersam, M. C. Sorting carbon nanotubes by electronic structure using density differentiation. *Nat. Nanotechnol.* **2006**, *1*, 60–65.
[16] Bakshi, S. R.; Lahiri, D.; Agarwal, A. Carbon nanotube reinforced metal matrix composites—A review. *Int. Mater. Rev.* **2010**, *55*, 41–64.
[17] García-Amorós, J.; Velasco, D. Recent advances towards azobenzene-based light-driven real-time information-transmitting materials. *Beilstein J. Org. Chem.* **2012**, *8*, 1003–1017.
[18] Ikeda, T.; Tsutsumi, O. Optical switching and image storage by means of azobenzene liquid-crystal films. *Science* **1995**, *268*, 1873–1875.
[19] Ichimura, K. Photoalignment of liquid-crystal systems. *Chem. Rev.* **2000**, *100*, 1847–1874.
[20] Yu, F. G.; Tu, Z. D.; Yang, S. J.; Xia, Y. Deposition of polymer-free and locally aligned semiconducting carbon nanotube networks via a vapor-mediated marangoni effect for high-performance field-effect transistors. *ACS Appl. Electron. Mater.* **2025**, *7*, 7388–7395.
[21] Ikawa, T.; Hoshino, F.; Matsuyama, T.; Takahashi, H.; Watanabe, O. Molecular-shape imprinting and immobilization of biomolecules on a polymer containing azo dye. *Langmuir* **2006**, *22*, 2747–2753.
[22] Kang, H. S.; Yang, S. Photopatterning via photofluidization of azobenzene polymers. *Light: Adv. Manuf.* **2022**, *3*, 3.
[23] Ruiz-Lopez, M. F.; Francisco, J. S.; Martins-Costa, M. T. C.; Anglada, J. M. Molecular reactions at aqueous interfaces. *Nat. Rev. Chem.* **2020**, *4*, 459–475.
[24] Feldmann, D.; Maduar, S. R.; Santer, M.; Lomadze, N.; Vinogradova, O. I.; Santer, S. Manipulation of small particles at solid liquid interface: Light-driven diffusioosmosis. *Sci. Rep.* **2016**, *6*, 36443.
[25] Gu, J. T.; Han, J.; Liu, D.; Yu, X. Q.; Kang, L. X.; Qiu, S.; Jin, H. H.; Li, H. B.; Li, Q. W.; Zhang, J. Solution-processable high-purity semiconducting swcnts for large-area fabrication of high-performance thin-film transistors. *Small* **2016**, *12*, 4993–4999.
[26] Yang, Y. J.; Ding, L.; Han, J.; Zhang, Z. Y.; Peng, L. M. High-performance complementary transistors and medium-scale integrated circuits based on carbon nanotube thin films. *ACS Nano* **2017**, *11*, 4124–4132.
[27] Yoon, J.; Lim, M.; Choi, B.; Kim, D. M.; Kim, D. H.; Kim, S.; Choi, S. J. Determination of individual contact interfaces in carbon nanotube network-based transistors. *Sci. Rep.* **2017**, *7*, 5453.
[28] Zhao, J.; Shen, L. J.; Liu, F.; Zhao, P.; Huang, Q.; Han, H.; Peng, L. M.; Liang, X. L. Quality metrology of carbon nanotube thin films and its application for carbon nanotube-based electronics. *Nano Res.* **2020**, *13*, 1749–1755.
[29] Tian, B. Y.; Liang, X. L.; Yan, Q. P.; Zhang, H.; Xia, J. Y.; Dong, G. D.; Peng, L. M.; Xie, S. S. Wafer scale fabrication of carbon nanotube thin film transistors with high yield. *J. Appl. Phys.* **2016**, *120*, 034501.
[30] Xiang, L.; Xia, F.; Zhang, H.; Liu, Y. D.; Liu, F.; Liang, X. L.; Hu, Y. F. Wafer-scale high-yield manufacturing of degradable electronics for environmental monitoring. *Adv. Funct. Mater.* **2019**, *29*, 1905518.
[31] Kim, J.; Hong, D.; Lee, H.; Shin, Y.; Park, S.; Khang, Y.; Lee, M.; Hong, S. Large-scale assembly of pristine semiconducting carbon nanotube network-based devices exhibiting intrinsic characteristics. *J. Phys. Chem. C* **2013**, *117*, 19721–19728.
[32] Liu, H. Y.; Zhang, P. P.; Cao, X. M.; Zhang, Y.; He, J. P.; Zhu, M. G.; Xiao, M. M.; Zhang, Z. Y. Long-channel effects in randomly oriented carbon nanotube thin film transistors. *Adv. Electron. Mater.* **2025**, *11*, 2400660.
[33] Sun, D. M.; Timmermans, M. Y.; Tian, Y.; Nasibulin, A. G.; Kauppinen, E. I.; Kishimoto, S.; Mizutani, T.; Ohno, Y. Flexible high-performance carbon nanotube integrated circuits. *Nat. Nanotechnol.* **2011**, *6*, 156–161.
[34] Xia, J. Y.; Zhao, J.; Meng, H.; Huang, Q.; Dong, G. D.; Zhang, H.; Liu, F.; Mao, D. F.; Liang, X. L.; Peng, L. M. Performance enhancement of carbon nanotube thin film transistor by yttrium oxide capping. *Nanoscale* **2018**, *10*, 4202–4208.